JACS
JOURNAL OF THE AMERICAN CHEMICAL SOCIETY
pubs.acs.org/JACS
Article

Fast-Switching Vis–IR Electrochromic Covalent Organic Frameworks

Derya Bessinger, Katharina Muggli, Michael Beetz, Florian Auras,* and Thomas Bein*

Cite This: J. Am. Chem. Soc. 2021, 143, 7351–7357

ABSTRACT: Electrochromic coatings are promising for applications in smart windows or energy-efficient optical displays. However, classical inorganic electrochromic materials such as WO_3 suffer from low coloration efficiency and slow switching speed. We have developed highly efficient and fast-switching electrochromic thin films based on fully organic, porous covalent organic frameworks (COFs). The low band gap COFs have strong vis–NIR absorption bands in the neutral state, which shift significantly upon electrochemical oxidation. Fully reversible absorption changes by close to 3 OD can be triggered at low operating voltages and low charge per unit area. Our champion material reaches an electrochromic coloration efficiency of 858 cm^2 C^{-1} at 880 nm and retains >95% of its electrochromic response over 100 oxidation/reduction cycles. Furthermore, the electrochromic switching is extremely fast with response times below 0.4 s for the oxidation and around 0.2 s for the reduction, outperforming previous COFs by at least an order of magnitude and rendering these materials some of the fastest-switching frameworks to date. This combination of high coloration efficiency and very fast switching reveals intriguing opportunities for applications of porous organic electrochromic materials.

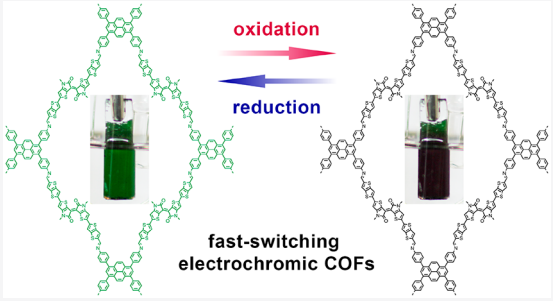

INTRODUCTION

Since their first development in 2005, covalent organic frameworks (COFs) have emerged into a very active research field of tailor-made functional nanostructures.[1−3] Constructed from rigid organic building blocks, COFs combine high crystallinity with a precisely defined porosity and large internal surface area.[4−6] A wide range of functional building blocks enable the design of bespoke networks with well-defined catalytic, optical, and electronic properties.[7−11]

Electrochromism describes reversible color changes of a material in response to an external electronic stimulus. Electrochromic materials have been applied in smart windows, optical displays, and molecular imaging.[12−14] In addition to well-established inorganic electrochromic materials such as WO_3, research focuses increasingly on organic molecular compounds and polymers.[15−17] Organic materials offer higher coloration efficiencies and better tunability owing to their broad range of possible chemical modifications, while the higher diffusion rates of charge-compensating counterions allow for faster switching times.[18,19]

Due to their permanent porosity on a molecular length scale, every building block throughout a COF domain can be brought into contact with an electrolyte, enabling very fast and efficient electrochromic switching. However, first examples of electrochromic COFs based on triphenylamine dyes have not yet reached their full potential, as they show only moderate coloration efficiencies and switching speeds.[20,21]

Here we present a series of fast-switching electrochromic 2D-COFs with panchromatic UV–vis–IR response and high coloration efficiency. Key to this performance is our linker design strategy where we combine a central thienoisoindigo moiety with more electron-rich units while fully retaining its favorable stacking interactions (Figure 1). This donor–acceptor–donor electronic setup promotes intramolecular charge transfer, leading to strong light absorption across the visible and near IR regions and an increased sensitivity of the absorption spectra toward electrochemical oxidation. COFs constructed from the new building blocks are highly crystalline frameworks with large one-dimensional pores for optimal accessibility of every building block throughout the material. Oriented COF thin films of the best-performing framework are stable over at least 200 oxidation/reduction cycles. They retain >95% of their electrochromic response over 100 cycles, show very rapid switching with response times below 0.4 s (oxidation) and around 0.2 s (reduction), and have coloration efficiencies of up to 858 cm^2 C^{-1}.

RESULTS

In order to maximize the electrochromic response across the visible and near-infrared (NIR) spectral regions, we constructed building blocks with a donor–acceptor–donor (D–A–D) electronic configuration. This design not only provides a sufficiently small band gap to push the absorption onset well

Received: November 27, 2020
Published: March 16, 2021

https://doi.org/10.1021/jacs.0c12392
J. Am. Chem. Soc. 2021, 143, 7351–7357

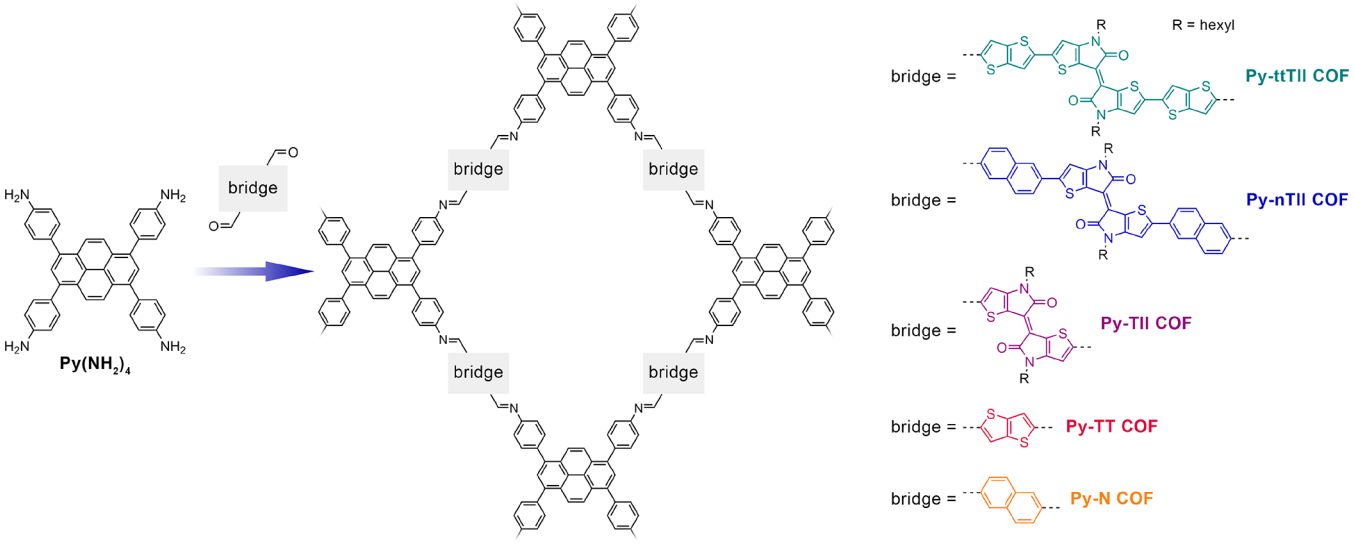

Figure 1. Construction of the new thienoisoindigo COFs and the Py-TT and Py-N COF reference materials. The co-condensation of the linear dicarboxaldehydes with the pyrene tetraaniline yields a series of isostructural frameworks with a pseudosquare geometry and slip-stacked 2D layers.

into the NIR (Supporting Information (SI), Figure S4) but also renders the charge-transfer (CT) and $\pi-\pi^*$ transitions very sensitive to electronic changes such that significant electrochromic response can be expected over a wide spectral range.[18,22−24] We chose the highly electron-deficient thienoisoindigo (TII) unit as the acceptor and combined it with the more electron-rich thienothiophene (TT) or naphthalene (N) donors, yielding the extended, NIR-absorbing ttTII$(CHO)_2$ and nTII$(CHO)_2$ building blocks, respectively (Figure 1). For comparison purposes, we also constructed the dicarboxaldehyde building blocks of the individual components (TII, TT, and N).

For COF construction we selected the well-established pyrene tetraaniline (Py$(NH_2)_4$) as the tetradentate counterpart. This building block is known to generate exceptionally crystalline and stable 2D-COFs with a broad range of linear linkers and, most importantly, is compatible with heteroaromatic moieties where strong electrostatic interactions enforce slip-stacked arrangements.[25−27] Moreover, the pyrene building block enables the synthesis of very well-oriented COF films on a variety of substrates.[28,29]

The Py-ttTII, Py-nTII, Py-TII, Py-TT, and Py-N COFs were synthesized under solvothermal conditions with aqueous acetic acid as the catalyst (see the SI, Section B for experimental details). The isoreticular COFs feature a pseudosquare geometry with slip-stacked 2D layers.

When synthesized as a bulk material, the Py-ttTII COF is a dark green powder. Its powder X-ray diffraction pattern exhibits a series of sharp reflections with only minimal background, confirming the formation of a highly crystalline framework (Figure 2a). Rietveld refinement carried out in the monoclinic space group $C2/m$ and using the structure model shown in Figure 2b provides a very good fit to the experimental pattern. The refined lattice parameters are $a = 6.33 \pm 0.02$ nm, $b = 5.89 \pm 0.02$ nm, $c = 0.39 \pm 0.02$ nm, and $\beta = 60 \pm 5°$. Due to the large number of atoms per unit cell and the inherent flexibility of the COF backbone and alkyl chains, it is not possible to refine individual atom positions. Thus, slight differences between the structure model and the actual COF structure are unavoidable, causing the deviations in intensity observed for some of the higher-index reflections.

While the refinement of individual atoms is not possible, the data quality is sufficient to refine the overall orientation of the alkyl chains. In the case of the Py-ttTII COF, the alkyl chains were found to extend straight into the pores, creating a shamrock-shaped pore cross section with wall-to-wall distances of 3.5 and 2.1 nm without and with alkyl chains, respectively (Figure 2c). This configuration is very similar to the geometries found in molecular crystals of thienoisoindigos with linear alkyl chains and is further supported by gas sorption analysis (see below).[30,31]

The nitrogen sorption isotherm recorded at 77 K exhibits a type IVb isotherm shape with a sharp step at $p/p_0 = 0.24$, confirming the mesoporosity of the framework (Figure 2d).[32] Analysis of the isotherm using the quenched solid density functional theory (QSDFT) method and an equilibrium model for cylindrical pores yields a bimodal pore size distribution (PSD). Bimodal PSDs have been observed previously for alkyl-containing COFs and are the result of the QSDFT method trying to describe a noncylindrical pore shape.[27] The maxima at 2.3 and 3.4 nm are in very good agreement with the wall-to-wall distances with and without alkyl chains, respectively, and further confirm the shamrock-shaped pore cross section with two predominant diagonals. The Py-ttTII COF has a Brunauer−Emmett−Teller (BET) surface area of 1370 $m^2\ g^{-1}$ with a total pore volume of 0.85 $cm^3\ g^{-1}$. The experimental surface area is about 60% of the Connolly surface area calculated from the idealized structure model. This reduction in porosity is frequently observed for alkyl-chain containing COFs and is mainly attributed to the enhanced trapping of oligomers due to the complex pore shape.[27,33] However, at 60% of the theoretical porosity, the accessibility throughout the framework is expected to be sufficient for efficient electrochemical switching (see below).

High-resolution transmission electron microscopy (TEM) images reveal the nanocrystalline morphology of the Py-ttTII COF powder with domain sizes of 50−100 nm (Figure 2e). Crystallites that are oriented with their crystallographic c-axis (i.e., along the pores) parallel to the viewing direction confirm the pseudosquare geometry with a periodicity of 4.0 nm, which is in excellent agreement with the refined structure model.

https://doi.org/10.1021/jacs.0c12392
J. Am. Chem. Soc. 2021, 143, 7351−7357

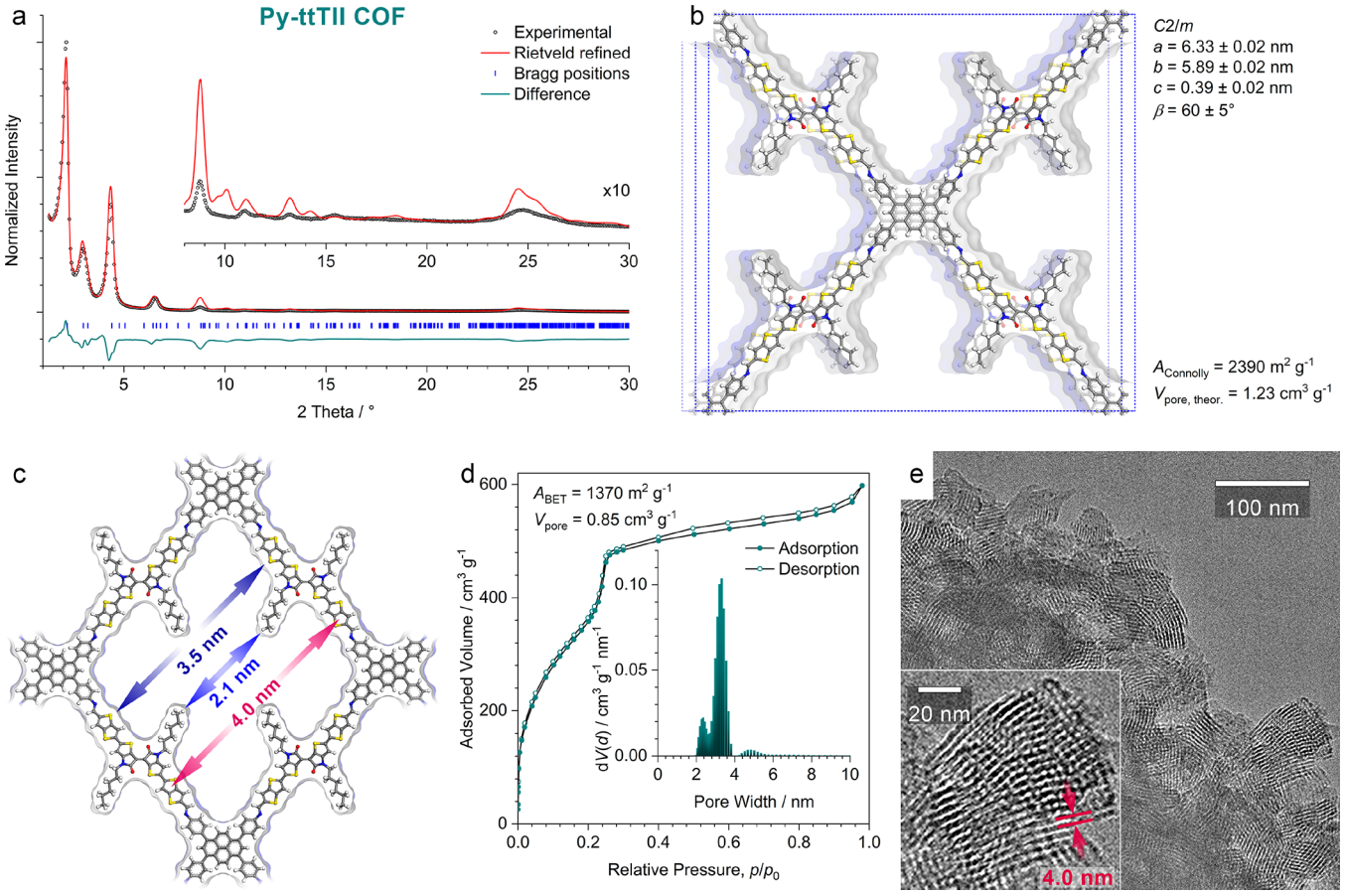

Figure 2. Structure analysis of the Py-ttTII COF. (a) Experimental PXRD pattern of the Py-ttTII COF bulk material (black dots). Rietveld refinement (red line) using the monoclinic (space group *C*2/*m*) structure model displayed in (b) provides a good fit with only minor differences between the experimental and refined patterns (green line) arising mainly from the flexibility of the alkyl chains. R_{wp} = 12.3%, R_p = 20.9%. Bragg positions are indicated by blue ticks. Inset: Magnified view of the $2\theta > 8°$ region. (b) The Rietveld-refined structure model of the Py-ttTII COF viewed perpendicular to the crystallographic *a*–*b* plane. The COF has a pseudosquare geometry with slip-stacked layers. The structure is highly porous with a Connolly surface area of 2390 $m^2 g^{-1}$ and a pore volume of 1.23 $cm^3 g^{-1}$. (c) Illustration of the pore structure of the COF viewed along the *c*-axis. The structure refinement indicates that in this COF the alkyl chains extend relatively straight into the pores, producing a shamrock-shaped pore cross section. The wall-to-wall distances (blue arrows) are 2.1 and 3.5 nm including and excluding the alkyl chains, respectively. The periodicity of the COF in this orientation is 4.0 nm (red arrows). (d) Nitrogen sorption isotherm recorded at 77 K. Inset: Fitting the isotherm with a QSDFT equilibrium model for cylindrical pores produces a bimodal pore size distribution (PSD) with peaks at 2.3 and 3.4 nm. These values are in good agreement with the wall-to-wall distances including and excluding the alkyl chains derived from the refined structure model, confirming the shamrock-shaped pore cross section. (e) High-resolution TEM image of a Py-ttTII COF bulk powder sample showing crystallites of approximately 50 nm diameter. Inset: A crystallite viewed along the pores (i.e., along the crystallographic *c*-axis) showing a periodicity of 4.0 nm in excellent agreement with the structure model.

The naphthalene-containing Py-nTII COF has a very similar structure and features the same shamrock-shaped pore cross section (SI, Figure S2-1). In contrast, due to the shorter TII(CHO)$_2$ building block, the alkyl chains of the Py-TII COF cannot extend straight into the pore, but are forced to collapse onto the pore walls (SI, Figures S2-2, S2-3). Hence, this COF has significantly narrower pores with a single maximum in the corresponding PSD. The Py-N and Py-TT COFs are highly crystalline frameworks with very similar overall topology but relatively small diamond-shaped pores (SI, Figure S2-5).[28]

For the electrochemistry and spectroelectrochemistry experiments, oriented COF thin films were grown on transparent and conductive indium tin oxide (ITO) coated glass (Py-ttTII, Py-TII, Py-TT, and Py-N COFs) or 10 nm Au on glass (Py-nTII COF) substrates using modified solvothermal protocols (see the SI, section B for details).

2D grazing-incidence wide-angle X-ray scattering (GIWAXS) measurements confirm that the COF films are crystalline and strongly textured (Figure 3a and SI, Figure S5). For all COFs, the *hk*0 reflections show the highest intensity close to the sample horizon, indicating a preferred orientation of the *a*–*b* plane parallel to the substrate surface. Consistently, the intensity of the 001 and other low-index *hk*1 reflections is concentrated within a 60° segment centered at $q_x = 0/q_z = 18$ nm^{-1}. This preferential orientation is highly desired, as the COF pores extend toward the film surface and are fully accessible.

The optical properties of the thienoisoindigo COFs are largely dominated by the strong absorption features of the ttTII, nTII, and TII building blocks (SI, Figure S4). The higher-energy absorption bands between 350 and 500 nm can be attributed to π–π^* transitions, while the longer-wavelength absorption is due to intramolecular charge transfer (ICT) between the electron-rich and -deficient moieties of the building blocks.[23,34] Both π–π^* and ICT bands appear red-shifted and broadened compared to the respective building blocks due to aggregation

https://doi.org/10.1021/jacs.0c12392
J. Am. Chem. Soc. 2021, 143, 7351–7357

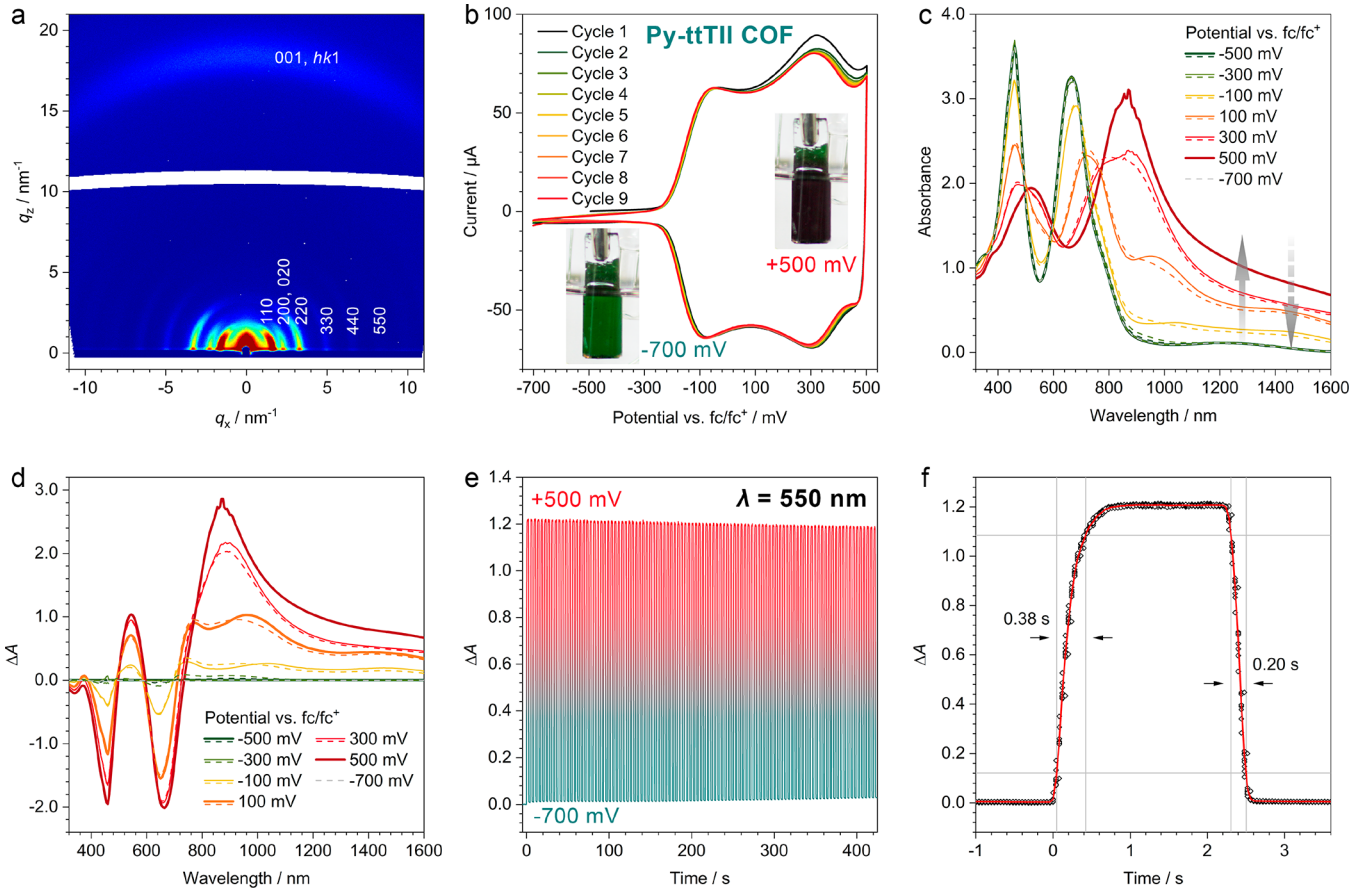

Figure 3. Electrochromism of Py-ttTII COF thin films. (a) GIWAXS pattern of a 430 nm thick Py-ttTII COF film grown on ITO/glass. Color scaling is logarithmic. The intensities of the *hk*0 reflections are concentrated directly above the sample horizon, confirming the anticipated strong texture with a predominant orientation of crystallites with their *a*−*b* plane parallel to the substrate surface. The 001 and other low-index *hk*1 reflections form an arc with the highest intensity in the middle segment close to the substrate normal. (b) Cyclic voltammetry scans of a Py-ttTII film on ITO/glass recorded at a scan rate of 20 mV s^{-1} in a three-electrode setup. The COF shows two very well-defined oxidation waves at −100 and +300 mV vs fc/fc$^+$, respectively, with negligible drift over nine oxidation/reduction cycles. Insets: Photographs of the COF film in the neutral (−700 mV) and oxidized (+500 mV) states. (c) Spectroelectrochemical characterization of a Py-ttTII COF film. UV−vis−NIR spectra are recorded at increasing (oxidation; solid lines) and decreasing (reduction; dashed lines) potentials. The electrochromic color changes are fully reversible with only minimal hysteresis. After reduction back to the neutral state (−700 mV; gray dashed line), the spectrum is indistinguishable from the initial spectrum (green). (d) Plot of the absorption difference between the spectra shown in (c) after stepwise oxidation and the initial spectrum. The first oxidation step produces an absorption band at 1000 nm (orange line), which is replaced by an even stronger band at 900 nm after the second oxidation step (dark red). The emergence of the new absorption bands is accompanied by two strong bleach bands that correspond to the absorption of the neutral Py-ttTII COF at 450 and 650 nm. (e) Electrochromic switching stability over 100 oxidation/reduction cycles. The applied potential is switched between −700 and +500 mV with 2 s dwell time after each potential step. Upon oxidation, the absorbance at 550 nm changes by 1.2 OD with only minimal drift (<5%) over 100 cycles. (f) Switching speed at 550 nm extracted from ten oxidation/reduction cycles (symbols: data points, red line: average). The electrochromic response of the Py-ttTII COF film is very fast with 0.38 s for the oxidation and 0.20 s for the reduction, determined between 10% and 90% Δ*A* thresholds.

effects across the closely packed, slip-stacked layers in the COF.[35]

In order to study the electrochromic behavior of our COFs, we integrated the COF thin film coated electrodes in a three-electrode electrochemical setup with a Pt wire as the counter electrode and a Ag/AgCl reference electrode (see the SI, section A for details). 0.1 M tetrabutylammonium hexafluorophosphate ($TBAPF_6$) in acetonitrile was used as the electrolyte. The applied potentials were calibrated against the ferrocene fc/fc$^+$ redox couple.

Cyclic voltammetry (CV) scans of the Py-ttTII COF show two very well-defined oxidation waves at around −100 and +300 mV, respectively, which appear mirrored when the scan direction is reversed (Figure 3b). The respective anodic and cathodic peak positions are shifted by only about 20 mV, suggesting that the redox processes in the COF are fully reversible with fast electron transfer kinetics. The reversibility is further illustrated by the absence of any major drift or changes in curve shape during repeated redox cycles.

Electrochemical oxidation of the Py-ttTII COF film causes a gradual color change from initially dark green to black (SI, Figure S6-1). The corresponding UV−vis−NIR spectra recorded in 200 mV intervals reveal the progressive bleaching of the two main absorption bands of the neutral COF, accompanied by the appearance of a new feature around 550 nm and a massive absorption band in the near-infrared (Figures 3c,d). The first oxidation step (−100 to +100 mV) produces a spectral feature at 1000 nm, which is replaced by an even stronger absorption band around 900 nm after the second oxidation step. The spectral changes are fully reversible with

https://doi.org/10.1021/jacs.0c12392
J. Am. Chem. Soc. 2021, 143, 7351−7357

only minimal hysteresis. The spectrum recorded at −700 mV is indistinguishable from the initial spectrum of the neutral COF.

The charge density extracted from a 430 nm thick COF film during the oxidation scan is 0.0032 C cm^{-2}, which is very close to the theoretical charge density of 0.0030 C cm^{-2} calculated for the two-electron oxidation of every ttTII unit in the COF film (see the SI, section I). We thus can assign the two oxidation waves in the CV scans and the corresponding 1000 and 900 nm absorption features to the $ttTII^{+}$ and $ttTII^{2+}$ species, respectively.

The two-electron oxidation leads to very strong absorption and bleach bands (absorption changes of up to 2.8 OD) and requires only slightly more charge per unit area than the theoretical limit discussed above. Thus, the electrochromic color changes are highly efficient with coloration efficiencies (CEs) of 318 cm^2 C^{-1} at 550 nm, 620 cm^2 C^{-1} at 660 nm, and 858 cm^2 C^{-1} at 880 nm, respectively (see the SI, section I). These values are several times higher than the CEs of previously reported electrochromic COFs,[20,21] rendering the Py-ttTII COF, to the best of our knowledge, the most efficient electrochromic organic framework to date.[36,37]

In order to further investigate the stability and response times, we alternated the applied potential between +500 mV (oxidized COF) and −700 mV (neutral COF). The Py-ttTII COF retains >95% of its initial electrochromic response over 100 oxidation/reduction cycles (Figure 3e and SI, Figure S7-1) and >85% over 200 cycles (SI, Figure S7-3). Furthermore, the framework crystallinity remains unaffected during these experiments. GIWAXS patterns of the COF film before and after 200 oxidation/reduction cycles are virtually identical (SI, Figure S5-1).

The response to step changes in the applied potential is extremely fast with response times of 0.38 s for the oxidation (coloration) and 0.2 s for the reduction (bleaching) at 550 nm (Figure 3f). Response times at 660 and 900 nm are similarly fast (SI, Figure S7-1e). To the best of our knowledge, the Py-ttTII COF is the fastest electrochromic framework to date, outcompeting published COFs and inorganic competitors such as WO_3 by more than an order of magnitude.[20,21,38]

As an illustration for a potential application of our electrochromic COFs, we employed a Py-ttTII COF film as an electrochromic window that can rapidly switch between transmitting (neutral COF) and blocking (oxidized COF) light from a green LED. A video of this is included as Supporting Information.

The electronically and topologically very similar Py-nTII COF shows an overall comparable electrochromic performance, but with slightly less defined oxidation and reduction waves, and weaker coloring due to the reduced film thickness (SI, Figure S6-2). Owing to their more electron-deficient and/or wider band gap building blocks, the Py-TII, Py-TT, and Py-N COFs require more positive potentials for oxidation (SI, Figures S6-3, S6-4, S6-5). Moreover, the color changes are much less pronounced and there is significant drift in the CV curves.

DISCUSSION

Comparing the five electrochromic COFs, we can formulate a set of design rules:

(I) Response and coloration efficiency critically depend on a building block design that combines high extinction coefficients with significant spectral differences between the neutral building block and its oxidized forms. The D−A−D electronic configuration of the ttTII and nTII building blocks has proven to be very efficient in fulfilling both criteria.

(II) Framework stability during repeated oxidation/reduction seems to depend on two factors. There is a general trend that for a given linker length the more rigid building blocks generate more robust frameworks. This factor works in favor of the flat and almost linear ttTII building block over the slightly nonplanar, more flexible nTII and the angled TII. Moreover, stability over repeated electrochromic switching cycles seems to depend critically on the pore size. The COF pores need to be sufficiently large to accommodate the counterions required for overall charge neutrality (i.e., four counterions per pore and COF layer for the two-electron oxidation of every bridge unit). They must also enable fast diffusion of electrolyte ions into and out of the pores during the electrochemical oxidation and reduction. Among the frameworks in this study, the Py-ttTII and Py-nTII COFs fulfill this criterion, whereas the smaller-pore COFs show significant drift during repeated CV scans, likely due to a buildup of ions in the pores.

(III) Rapid response requires unimpeded diffusion of ions in the pores as well as electronic connectivity throughout the COF film. The Py-ttTII COF films have a unique pillar-like morphology (SI, Figure S5-1c). Every pillar appears to be a continuous COF nanocrystal, ensuring best possible electronic coupling to the ITO electrode and uninterrupted pores for fast electrolyte diffusion.

CONCLUSION

We have developed highly efficient, fast-switching and stable electrochromic covalent organic frameworks based on modified thienoisoindigo building blocks. With a donor−acceptor−donor electronic setup, the low band gap COFs have strong vis−NIR absorption bands in the neutral state, which shift significantly upon electrochemical oxidation. Absorption changes by close to 3 OD can be triggered at low operating voltages and are fully reversible. The champion Py-ttTII COF reaches an electrochromic coloration efficiency of 858 cm^2 C^{-1} at 880 nm and retains >95% of its electrochromic response over 100 oxidation/reduction cycles. Furthermore, the electrochromic switching of our oriented COF films is extremely fast with response times below 0.4 s for the oxidation and around 0.2 s for the reduction, outperforming previous COFs by at least an order of magnitude and rendering these materials, to the best of our knowledge, the fastest-switching frameworks to date.

ASSOCIATED CONTENT

Supporting Information

The Supporting Information is available free of charge at https://pubs.acs.org/doi/10.1021/jacs.0c12392.

Experimental methods, synthetic procedures, structure analysis, and additional spectroscopic data (PDF)

Video showing the electrochromic switching (MPG)

AUTHOR INFORMATION

Corresponding Authors

Thomas Bein − *Department of Chemistry and Center for NanoScience (CeNS), University of Munich (LMU), 81377 Munich, Germany;* orcid.org/0000-0001-7248-5906; Email: bein@lmu.de

https://doi.org/10.1021/jacs.0c12392
J. Am. Chem. Soc. 2021, 143, 7351−7357

Florian Auras − *Cavendish Laboratory, University of Cambridge, CB3 0HE Cambridge, United Kingdom;* orcid.org/0000-0003-1709-4384; Email: fa355@cam.ac.uk

Authors

Derya Bessinger − *Department of Chemistry and Center for NanoScience (CeNS), University of Munich (LMU), 81377 Munich, Germany*

Katharina Muggli − *Department of Chemistry and Center for NanoScience (CeNS), University of Munich (LMU), 81377 Munich, Germany*

Michael Beetz − *Department of Chemistry and Center for NanoScience (CeNS), University of Munich (LMU), 81377 Munich, Germany*

Complete contact information is available at: https://pubs.acs.org/10.1021/jacs.0c12392

Notes

The authors declare no competing financial interest.

■ ACKNOWLEDGMENTS

The research leading to these results has received funding from the European Research Council under the European Union's Seventh Framework Programme (FP7/2007-2013/ERC Grant Agreement No. 321339). The authors acknowledge funding from the Deutsche Forschungsgemeinschaft (DFG, German Research Foundation) under Germany's Excellence Strategy − EXC 2089/1 − 390776260. The authors thank Markus Döblinger for the TEM characterization and Andre Mähringer and Roman Guntermann for the GIWAXS measurements.

■ REFERENCES

(1) Côte, A. P.; Benin, A. I.; Ockwig, N. W.; O'Keeffe, M.; Matzger, A. J.; Yaghi, O. M. Porous, Crystalline, Covalent Organic Frameworks. *Science* **2005**, *310*, 1166−1170.

(2) Jin, E.; Asada, M.; Xu, Q.; Dalapati, S.; Addicoat, M. A.; Brady, M. A.; Xu, H.; Nakamura, T.; Heine, T.; Chen, Q.; Jiang, D. Two-dimensional sp2 carbon−conjugated covalent organic frameworks. *Science* **2017**, *357*, 673−676.

(3) Ma, T.; Kapustin, E. A.; Yin, S. X.; Liang, L.; Zhou, Z.; Niu, J.; Li, L.-H.; Wang, Y.; Su, J.; Li, J.; Wang, X.; Wang, W. D.; Wang, W.; Sun, J.; Yaghi, O. M. Single-crystal x-ray diffraction structures of covalent organic frameworks. *Science* **2018**, *361*, 48−52.

(4) Xu, H.; Gao, J.; Jiang, D. Stable, crystalline, porous, covalent organic frameworks as a platform for chiral organocatalysts. *Nat. Chem.* **2015**, *7*, 905−912.

(5) Li, R. L.; Flanders, N. C.; Evans, A. M.; Ji, W.; Castano, I.; Chen, L. X.; Gianneschi, N. C.; Dichtel, W. R. Controlled growth of imine-linked twodimensional covalent organic framework nanoparticles. *Chem. Sci.* **2019**, *10*, 3796−3801.

(6) Ascherl, L.; Sick, T.; Margraf, J. T.; Lapidus, S. H.; Calik, M.; Hettstedt, C.; Karaghiosoff, K.; Döblinger, M.; Clark, T.; Chapman, K. W.; Auras, F.; Bein, T. Molecular docking sites designed for the generation of highly crystalline covalent organic frameworks. *Nat. Chem.* **2016**, *8*, 310−316.

(7) Spitler, E. L.; Dichtel, W. R. Lewis acid-catalysed formation of two-dimensional phthalocyanine covalent organic frameworks. *Nat. Chem.* **2010**, *2*, 672−677.

(8) Dogru, M.; Handloser, M.; Auras, F.; Kunz, T.; Medina, D.; Hartschuh, A.; Knochel, P.; Bein, T. A Photoconductive Thienothiophene-Based Covalent Organic Framework Showing Charge Transfer Towards Included Fullerene. *Angew. Chem., Int. Ed.* **2013**, *52*, 2920−2924.

(9) Calik, M.; Auras, F.; Salonen, L. M.; Bader, K.; Grill, I.; Handloser, M.; Medina, D. D.; Dogru, M.; Löbermann, F.; Trauner, D.; Hartschuh, A.; Bein, T. Extraction of Photogenerated Electrons and Holes from a Covalent Organic Framework Integrated Heterojunction. *J. Am. Chem. Soc.* **2014**, *136*, 17802−17807.

(10) Stegbauer, L.; Schwinghammer, K.; Lotsch, B. V. A Hydrazone-based Covalent Organic Framework for Photocatalytic Hydrogen Production. *Chem. Sci.* **2014**, *5*, 2789−2793.

(11) Wang, X.; Chen, L.; Chong, S. Y.; Little, M. A.; Wu, Y.; Zhu, W.-H.; Clowes, R.; Yan, Y.; Zwijnenburg, M. A.; Sprick, R. S.; Cooper, A. I. Sulfone-containing covalent organic frameworks for photocatalytic hydrogen evolution from water. *Nat. Chem.* **2018**, *10*, 1180−1189.

(12) Rauh, R. D. Electrochromic windows: an overview. *Electrochim. Acta* **1999**, *44*, 3165−3176.

(13) Cheng, C.-P.; Kuo, Y.; Chou, C.-P.; Cheng, C.-H.; Teng, T. P. Performance improvement of electrochromic display devices employing micro-size precipitates of tungsten oxide. *Appl. Phys. A: Mater. Sci. Process.* **2014**, *116*, 1553−1559.

(14) Wu, L.; Sun, Y.; Sugimoto, K.; Luo, Z.; Ishigaki, Y.; Pu, K.; Suzuki, T.; Chen, H.-Y.; Ye, D. Engineering of Electrochromic Materials as Activatable Probes for Molecular Imaging and Photodynamic Therapy. *J. Am. Chem. Soc.* **2018**, *140*, 16340−16352.

(15) Knott, E. P.; Craig, M. R.; Liu, D. Y.; Babiarz, J. E.; Dyer, A. L.; Reynolds, J. R. A minimally coloured dioxypyrrole polymer as a counter electrode material in polymeric electrochromic window devices. *J. Mater. Chem.* **2012**, *22*, 4953−4962.

(16) Gu, H.; Ming, S.; Lin, K.; Chen, S.; Liu, X.; Lu, B.; Xu, J. Isoindigo as an electron-deficient unit for high-performance polymeric electrochromics. *Electrochim. Acta* **2018**, *260*, 772−782.

(17) Arockiam, J. B.; Son, H.; Han, S. H.; Balamurugan, G.; Kim, Y.-H.; Park, J. S. Iron Phthalocyanine Incorporated Metallo-Supramolecular Polymer for Superior Electrochromic Performance with High Coloration Efficiency and Switching Stability. *ACS Appl. Energy Mater.* **2019**, *2*, 8416−8424.

(18) Beaujuge, P. M.; Ellinger, S.; Reynolds, J. R. The donor−acceptor approach allows a black-to-transmissive switching polymeric electrochrome. *Nat. Mater.* **2008**, *7*, 795−799.

(19) Sapp, S. A.; Sotzing, G. A.; Reynolds, J. R. High Contrast Ratio and Fast-Switching Dual Polymer Electrochromic Devices. *Chem. Mater.* **1998**, *10*, 2101−2108.

(20) Hao, Q.; Li, Z.-J.; Lu, C.; Sun, B.; Zhong, Y.-W.; Wan, L.-J.; Wang, D. Oriented Two-Dimensional Covalent Organic Framework Films for Near-Infrared Electrochromic Application. *J. Am. Chem. Soc.* **2019**, *141*, 19831−19838.

(21) Yu, F.; Liu, W.; Ke, S.-W.; Kurmoo, M.; Zuo, J.-L.; Zhang, Q. Electrochromic two-dimensional covalent organic framework with a reversible dark-to-transparent switch. *Nat. Commun.* **2020**, *11*, 5534.

(22) Beaujuge, P. M.; Amb, C. M.; Reynolds, J. R. Spectral Engineering in π-Conjugated Polymers with Intramolecular Donor-Acceptor Interactions. *Acc. Chem. Res.* **2010**, *43*, 1396−1407.

(23) Stalder, R.; Mei, J.; Reynolds, J. R. Isoindigo-Based Donor-Acceptor Conjugated Polymers. *Macromolecules* **2010**, *43*, 8348−8352.

(24) Ho, C.-C.; Chen, C.-A.; Chang, C.-Y.; Darling, S. B.; Su, W.-F. Isoindigo-based copolymers for polymer solar cells with efficiency over 7%. *J. Mater. Chem. A* **2014**, *2*, 8026−8032.

(25) Auras, F.; Ascherl, L.; Hakimioun, A. H.; Margraf, J. T.; Hanusch, F. C.; Reuter, S.; Bessinger, D.; Döblinger, M.; Hettstedt, C.; Karaghiosoff, K.; Herbert, S.; Knochel, P.; Clark, T.; Bein, T. Synchronized Offset Stacking: A Concept for Growing Large-Domain and Highly Crystalline 2D Covalent Organic Frameworks. *J. Am. Chem. Soc.* **2016**, *138*, 16703−16710.

(26) Keller, N.; Bessinger, D.; Reuter, S.; Calik, M.; Ascherl, L.; Hanusch, F. C.; Auras, F.; Bein, T. Oligothiophene-Bridged Conjugated Covalent Organic Frameworks. *J. Am. Chem. Soc.* **2017**, *139*, 8194−8199.

(27) Bessinger, D.; Ascherl, L.; Auras, F.; Bein, T. Spectrally Switchable Photodetection with Near-Infrared-Absorbing Covalent Organic Frameworks. *J. Am. Chem. Soc.* **2017**, *139*, 12035−12042.

(28) Ascherl, L.; Evans, E. W.; Hennemann, M.; Di Nuzzo, D.; Hufnagel, A. G.; Beetz, M.; Friend, R. H.; Clark, T.; Bein, T.; Auras, F.

Solvatochromic covalent organic frameworks. *Nat. Commun.* **2018**, *9*, 3802.
(29) Ascherl, L.; Evans, E. W.; Gorman, J.; Orsborne, S.; Bessinger, D.; Bein, T.; Friend, R. H.; Auras, F. Perylene-Based Covalent Organic Frameworks for Acid Vapor Sensing. *J. Am. Chem. Soc.* **2019**, *141*, 15693−15699.
(30) Hasegawa, T.; Ashizawa, M.; Matsumoto, H. Design and structure−property relationship of benzothienoisoindigo in organic field effect transistors. *RSC Adv.* **2015**, *5*, 61035−61043.
(31) Yoo, D.; Hasegawa, T.; Ashizawa, M.; Kawamoto, T.; Masunaga, H.; Hikima, T.; Matsumoto, H.; Mori, T. *N*-Unsubstituted thienoisoindigos: preparation, molecular packing and ambipolar organic field-effect transistors. *J. Mater. Chem. C* **2017**, *5*, 2509−2512.
(32) Cychosz, K. A.; Guillet-Nicolas, R.; García-Martínez, J.; Thommes, M. Recent advances in the textural characterization of hierarchically structured nanoporous materials. *Chem. Soc. Rev.* **2017**, *46*, 389−414.
(33) Matsumoto, M.; Dasari, R. R.; Ji, W.; Feriante, C. H.; Parker, T. C.; Marder, S. R.; Dichtel, W. R. Rapid, Low Temperature Formation of Imine-Linked Covalent Organic Frameworks Catalyzed by Metal Triflates. *J. Am. Chem. Soc.* **2017**, *139*, 4999−5002.
(34) Dutta, G. K.; Han, A.-R.; Lee, J.; Kim, Y.; Oh, J. H.; Yang, C. Visible-Near Infrared Absorbing Polymers Containing Thienoisoindigo and Electron-Rich Units for Organic Transistors with Tunable Polarity. *Adv. Funct. Mater.* **2013**, *23*, 5317−5325.
(35) Oleson, A.; Zhu, T.; Dunn, I. S.; Bialas, D.; Bai, Y.; Zhang, W.; Dai, M.; Reichman, D. R.; Tempelaar, R.; Huang, L.; Spano, F. C. Perylene Diimide-Based Hj- and hJ-Aggregates: The Prospect of Exciton Band Shape Engineering in Organic Materials. *J. Phys. Chem. C* **2019**, *123*, 20567−20578.
(36) Feng, J. f.; Liu, T. F.; Cao, R. An Electrochromic Hydrogen-Bonded Organic Framework Film. *Angew. Chem., Int. Ed.* **2020**, *59*, 22392−22396.
(37) Wade, C. R.; Li, M.; Dincă, M. Facile Deposition of Multicolored Electrochromic Metal−Organic Framework Thin Films. *Angew. Chem., Int. Ed.* **2013**, *52*, 13377−13381.
(38) Cai, G.; Cui, M.; Kumar, V.; Darmawan, P.; Wang, J.; Wang, X.; Eh, A. L.-S.; Qian, K.; Lee, P. S. Ultra-large optical modulation of electrochromic porous WO_3 film and the local monitoring of redox activity. *Chem. Sci.* **2016**, *7*, 1373−1382.

https://doi.org/10.1021/jacs.0c12392
J. Am. Chem. Soc. 2021, 143, 7351−7357